

Relaxed Conditional Image Transfer for Semi-supervised Domain Adaptation

Qijun Luo^{1*}, Zhili Liu^{2,3*}, Lanqing Hong³, Chongxuan Li^{4†}, Kuo Yang³,
Liyuan Wang⁴, Fengwei Zhou³, Guilin Li³, Zhenguo Li³, Jun Zhu^{4†}

¹Chinese University of Hong Kong, Shen Zhen, China

²The Hong Kong University of Science and Technology, China

³Huawei Noah's Ark Lab, China

⁴Dept. of Comp. Sci. & Tech., Institute for AI, THBI Lab, BNRist Center,
State Key Lab for Intell. Tech. & Sys., Tsinghua University, Beijing, China

Abstract

Semi-supervised domain adaptation (SSDA), which aims to learn models in a partially labeled target domain with the assistance of the fully labeled source domain, attracts increasing attention in recent years. To explicitly leverage the labeled data in both domains, we naturally introduce a conditional GAN framework to transfer images without changing the semantics in SSDA. However, we identify a label-domination problem in such an approach. In fact, the generator tends to overlook the input source image and only memorizes prototypes of each class, which results in unsatisfactory adaptation performance. To this end, we propose a simple yet effective Relaxed conditional GAN (Relaxed cGAN) framework. Specifically, we feed the image without its label to our generator. In this way, the generator has to infer the semantic information of input data. We formally prove that its equilibrium is desirable and empirically validate its practical convergence and effectiveness in image transfer. Additionally, we propose several techniques to make use of unlabeled data in the target domain, enhancing the model in SSDA settings. We validate our method on the well-adopted datasets: Digits, DomainNet, and Office-Home. We achieve state-of-the-art performance on DomainNet, Office-Home and most digit benchmarks in low-resource and high-resource settings.

1. Introduction

While deep neural networks (DNNs) have made remarkable progress on various visual tasks [15, 22, 41], they usually rely on a large amount of labeled data in model training.

*These authors contribute equally to this work. The work is done when Qijun Luo and Zhili Liu are interns in Huawei Noah's Ark Lab. † Corresponding authors: C. Li, email: chongxuanli1991@gmail.com, and J. Zhu, email: dcszj@mail.tsinghua.edu.cn.

However, it is often costly to collect extensive training data with labels for a new coming task. To alleviate the burden of data collection, domain adaptation (DA) methods aim to learn a model on a target domain with the assistance of a source domain in which sufficient annotated data are available [35]. Existing DA methods [9, 43, 42, 27, 4, 20] mainly focus on unsupervised settings, where labels are unavailable in the target domain. Some recent works, however, have shown that a few labeled data in the target domain could significantly boost the model performance [40, 31, 17]. Considering that it is usually acceptable to collect a few labeled data of a target task for performance improvement, semi-supervised domain adaptation (SSDA) attracts more and more attention in recent years, which investigates to learn models in a partially labeled target domain with fully labeled data from a related source domain [31, 17, 37].

Current SSDA methods mainly fall into two categories, namely, the feature-level adaptation and the pixel-level adaptation. For feature-level adaptation, most methods either learn an invariant representation across domains by minimizing certain discrepancy [46] or extract target discriminative features with source domain as regularization [39]. For pixel-level adaptation, the main idea is to transfer source domain images to the target domain's style, serving as data augmentation [17]. In this paper, we mainly focus on pixel-level SSDA methods, as it enjoys the advantages of more stable model training and higher inter-pretability as the transferred images can be visualized and re-used [5].

Among pixel-level adaptation, the cycle-consistency loss is a popular technique for image transformation [45, 16, 17, 33, 28, 26, 18]. Such an approach, however, often suffers from a major obstacle named label-inconsistency, in which the generated image's label is different from the input image [17, 33, 28]. To address this issue in SSDA, a straightforward and common way is to adopt a conditional

GAN to align the class-conditional distribution of generated image-label pairs. Nevertheless, we empirically show that such design meets a *label-domination* problem, in which the generator tends to neglect the source image’s information and only generates images according to the input label (see Fig. 2 for empirical evidence). Such an issue would result in unsatisfactory adaptation due to the ineffective usage of the source domain’s information.

To alleviate this issue, we propose **Relaxed conditional GAN** (Relaxed cGAN), where a source image is fed into the generator for adaptation *without* the label. The resulting generated image together with the true label of the input image needs to fool the conditional discriminator. In this way, the generator is enforced to learn useful features from the raw images and generate meaningful samples in the target domain. We show that the proposed method has provable theoretical equilibrium and practical convergence properties. Moreover, we empirically demonstrates satisfactory image quality in transformation (see Fig. 5).

We compare Relaxed cGAN to several strong baselines, including both feature-based ones [37, 46, 31, 32, 39] and pixel-based ones [17, 45], on the commonly used Digit and more challenging DomainNet and Office-Home datasets. We obtain state-of-the-art results on most Digit datasets and DomainNet. Digits are conducted in both low-resource and high-resource settings. Competitive results are also obtained on the Office-Home.

To summarize, our main contributions are:

- We identify the label-domination problem on a natural and widespread conditional GAN framework for SSDA.
- We propose Relaxed cGAN, with carefully designed modules and loss functions to address the label-domination problem and validate our intuition in both theory and practice. Besides, we propose a marginal loss to enhance Relaxed cGAN without affecting the theoretical results.
- We obtain promising results in various SSDA settings. As a pixel-level method, we obtain state-of-the-art performance on widely adopted Digit datasets and DomainNet, and competitive results on Office-Home.

2. Related Work

Unsupervised Domain Adaptation. Unsupervised domain adaptation (UDA) aims to transfer knowledge from a source domain to a totally unlabeled target domain. Existing UDA methods mainly fall into two categories. One is the feature-level UDA algorithms, which propose to learn a domain-invariant representation by minimizing certain discrepancy measurements. A lot of measurements are defined by maximum mean discrepancy [14, 38, 27], Wasserstein metric [1],

graph matching [6], and adversarial methods [9, 43]. Another category adapts to domains in pixel-level, transferring samples from the source domain to the target domain’s style [16, 5, 33, 7]. Such methods are mostly based on the cycle-consistency loss [45]. Although the UDA settings are widely considered, it is usually affordable to collect a few labeled data in the target domain to boost the model performance. Therefore, SSDA may become a more practical setting.

Semi-supervised Domain Adaptation. As mentioned above, the target domain may have partially labeled data in many applications, which is referred to as the SSDA setting. There are a few methods that explore the setting. In feature-level, [39] utilizes unlabeled target domain’s data by minimizing their distance with class prototypes through a min-max training. Other approaches include mapping samples into shared embedding [37] and greedily minimizing information entropy [46]. On the pixel space, [17] imposes a classifier to serve as a complementary discriminator. However, it doesn’t utilize the target domain unlabeled data well. In comparison, our Relaxed cGAN proposes to achieve better image transformation with the help of both the labeled and unlabeled data in the target domain, and eventually benefits the clarification accuracy.

3. A Preliminary Framework

We first formulate semi-supervised domain adaptation (SSDA) and introduce a preliminary framework based on conditional GAN [30] in Sec. 3.1. Then, we identify a *label-domination* problem of the framework in Sec. 3.2.

3.1. Settings and Framework

In the SSDA settings, the source domain contains a large set of labeled data $\mathcal{D}_s = \{(x_i^s, y_i^s)\}_{i=1}^{m_s}$. In the target domain, we have a small set of labeled data $\mathcal{D}_t = \{(x_i^t, y_i^t)\}_{i=1}^{m_t}$ and a large set of unlabeled data $\mathcal{D}_u = \{(x_i^u)\}_{i=1}^{m_u}$. Let $p_s(x, y)$, $p_t(x, y)$ and $p_u(x)$ denote the empirical distributions over \mathcal{D}_s , \mathcal{D}_t , and \mathcal{D}_u , respectively. $p_s(x)$ and $p_t(x)$ denote the marginal distributions of x with respect to $p_s(x, y)$ and $p_t(x, y)$, respectively.

To adapt to different domains, cycle consistency constraint is a popular technique. It transfers the image in the source domain to match the target domain’s style by ensuring that the generated image can be reconstructed back to the original one. The generated image accompanied by the original label can serve as the augmentation of annotated target images. However, when the domain shift is large, such an approach may encounter the label-inconsistency problem [16] where the label of the generated image is different from the input one. For instance, when transferring the image from SVHN [34] to MNIST [23], the original image of label “5” may be transferred to a target image of label “3”, as shown in Fig 1(b). This could happen because there



Figure 1: Label-inconsistency problem. Each odd column shows the input source images, and its next column are corresponding generated images in the target domain. CycleGAN suffers from the severe label-inconsistency problem in most cases.

does not exist any inductive bias that ensures the label consistency should be maintained during the transformation.

A natural way to address this issue is to impose conditional GAN [30] to transfer images so that the class-conditional distribution between generated images and target domain images can be aligned. Specifically, we design a preliminary framework which adopts a conditional generator and a conditional discriminator with the following loss:

$$\mathcal{L}_{GAN} = \mathbb{E}_{(x,y) \sim p_t(x,y)} [\log(D_T(x,y))] + \mathbb{E}_{(x,y) \sim p_s(x,y)} [\log(1 - D_T(G_{S \rightarrow T}(x,y), y))],$$

where $G_{S \rightarrow T}$ is the conditional generator from source to target. D_T is the conditional discriminator of the target domain, distinguishing whether the generated image accompanied by the input label is close to the desired joint distribution. For the ease of later discussion, we omit the loss of the opposite direction from target to source, which also contains a conditional generator and a conditional discriminator. To maintain the correlation between the source image and the generated image, we also apply conventional cycle consistency loss, which is formulated as

$$\mathcal{L}_{cycle} = \mathbb{E}_{(x,y) \sim p_s(x,y)} [|G_{T \rightarrow S}(G_{S \rightarrow T}(x,y), y) - x|] + \mathbb{E}_{(x,y) \sim p_t(x,y)} [|G_{S \rightarrow T}(G_{T \rightarrow S}(x,y), y) - x|],$$

where $|\cdot|$ is the L1 distance on reconstruction error. To train a classifier, we apply standard cross-entropy loss on both target annotated images and generated images. The corresponding loss is

$$\mathcal{L}_C = \mathbb{E}_{(x,y) \sim p_s(x,y)} [-\log(C(y|G_{S \rightarrow T}(x)))] + \mathbb{E}_{(x,y) \sim p_t(x,y)} [-\log(C(y|x))], \quad (1)$$

where $C(y|x)$ is the y_{th} class’s probability predicted by the classifier for image x .

The overall objective function of our preliminary framework would be

$$\mathcal{L} = \lambda_{GAN} \mathcal{L}_{GAN} + \lambda_{cycle} \mathcal{L}_{cycle} + \lambda_C \mathcal{L}_C,$$

where λ_{GAN} , λ_{cycle} , λ_C are the corresponding weight for these losses.

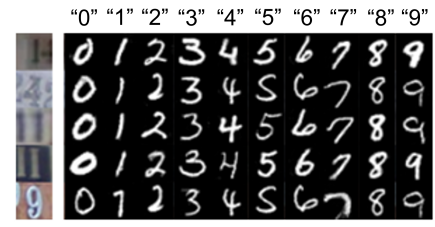


Figure 2: Label-domination problem. The generator receives images from the leftmost column, paired with each label from “0” to “9”. In the right part, the image in the i -th row and j -th column is the corresponding generated image of the i -th input image and label ‘ j ’. The output images are dominated by the input labels, showing no relationship with input images. More experiments demonstrating the existence of the label-domination problem can be seen in Appendix C.

3.2. The Label-domination Problem

While the preliminary method resolves the label-inconsistency problem, we argue that this approach meets a major obstacle, referred to as the *label-domination problem*, where the output of the conditional generator $G_{S \rightarrow T}(x,y)$ is dominated by the input label y and the information of the source domain data x is ignored. We empirically identify the existence of the label-domination problem by constructing a series of experiments on $\mathcal{S} \rightarrow \mathcal{M}$. As shown in Fig. 2, the left images and different labels are input to the conditional generator and the right-side images are the corresponding output. It shows that no matter what the input image is, the output will always follow the input label and show no correlation with the input images. Refer to Appendix C for ablation experiments that eliminate the effect of other factors including the network architectures, cycle consistency loss, and Spectral Normalization.

Intrinsically, the conditional discriminator in the target domain cannot avoid such a trivial solution. That is because the generator can simply memorize some prototypes in each class and only generate the corresponding prototype according to the input label to cheat the discriminator. Such a trivial solution ignores the information of the source image and thereby would result in a poor adaptation.

As quantitatively shown in row 3 of Table. 5, this preliminary approach has roughly the same classification accuracy as semi-supervised learning, which validates our intuition.

4. Method

We first present the proposed Relaxed cGAN framework to solve the label-domination problem in Sec. 4.1. We then analyze it in terms of the theoretical equilibrium and empirical convergence in Sec. 4.2. Finally, we present additional regularization to enhance the Relaxed cGAN framework for

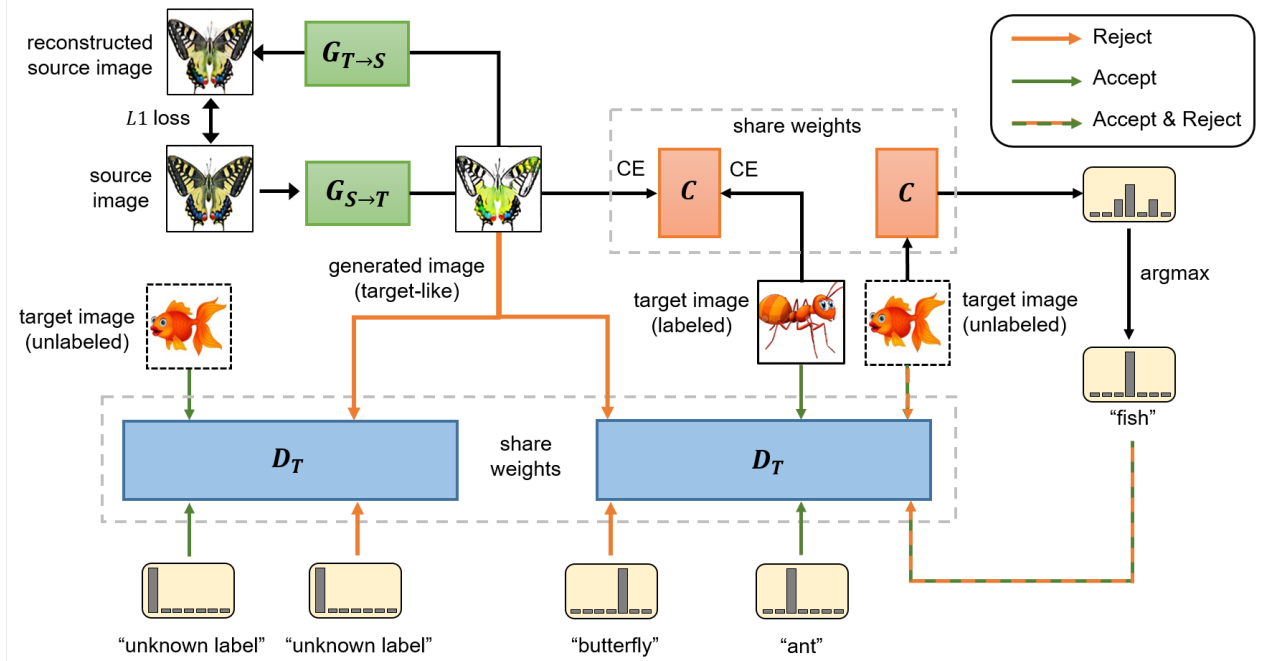


Figure 3: An overview of Relaxed cGAN. The discriminator takes image-label pairs as input while the generator takes source images as the only input, resolving both label inconsistency and label domination problem (see Sec. 4.1). The classifier is jointly trained with the generator and discriminator, ensuring a provable equilibrium (see Sec.4.2). Additionally, the discriminator accepts all real images in the target domain to leverage unlabeled data without changing the equilibrium (the left D_T , see Sec. 4.3). Note that the discriminator randomly accepts the image-label pairs from the classifier to augment the labeled sample pool (see Sec. 5.1).

SSDA in Sec. 4.3.

4.1. Relaxed cGAN for a Provable Equilibrium

The label-domination problem directly motivates our design of Relaxed cGAN. Our key intuition is that the source-domain image itself contains semantic information and therefore the label is not necessary to be included in the generator. Specifically, different from the preliminary approach, we feed images *without* labels to our generator for adaptation. Then we construct the image-label pairs with the generated images and the labels inherited from the ground truth of the input images. Such image-label pairs are used to fool the discriminator. By doing this, the generator is enforced to learn useful features from the raw images and generate meaningful samples in the target domain. Thus, the corresponding losses become

$$\begin{aligned} \mathcal{L}_{GAN} = & \mathbb{E}_{(x,y) \sim p_t(x,y)} [\log(D_T(x,y))] \\ & + \alpha \mathbb{E}_{(x,y) \sim p_s(x,y)} [\log(1 - D_T(G_{S \rightarrow T}(x), y))] \\ & + (1 - \alpha) \mathbb{E}_{x \sim p_u(x)} [\log(1 - D_T(x, C(x)))], \end{aligned} \quad (2)$$

and the cycle loss is

$$\begin{aligned} \mathcal{L}_{cycle} = & \mathbb{E}_{(x,y) \sim p_s(x,y)} [|G_{T \rightarrow S}(G_{S \rightarrow T}(x)) - x|] \\ & + \mathbb{E}_{(x,y) \sim p_t(x,y)} [|G_{S \rightarrow T}(G_{T \rightarrow S}(x)) - x|], \end{aligned}$$

where $C(x)$ is the classifier’s predicted class for image x . The third term and the loss weight of $(1 - \alpha)$ in \mathcal{L}_{GAN} is the adversarial training between the classifier and the discriminator. For simplicity we set $\alpha = \frac{1}{2}$ following [24]. They are used to guarantee our method for a provable Nash equilibrium, referring to the next section. Except for these factors, the main difference from the losses in the preliminary method is that the inputs to both generators are the images only, while the discriminator still receives the image-label pairs as input.

4.2. Theoretical and Empirical Analysis

We now analyze Relaxed cGAN in terms of theoretical equilibrium, practical convergence, and image transfer results.

Theoretical Equilibrium. We prove that the minimax game defined by Relaxed cGAN has a unique global equilibrium (under the non-parametric assumption [12]) that the generated joint distribution, the classifier distribution, and

the real target distribution are the same.

Formally, let $p_g(x, y)$ denote the joint distribution characterized by the image-label pairs of generated images and their original labels, $p_c(x, y)$ denote the distribution of image-label pairs constructed from the target domain images and the corresponding predictions by the classifier, and $p_t(x, y)$ denote the target domain joint distribution as mentioned in the Sec. 3.1 settings. We have the following theorem to show that our design theoretically has a desirable equilibrium. The detailed proof is given in Appendix A.

Theorem 1 *Under the non-parametric assumption, the equilibrium of $\tilde{\mathcal{L}}(C, G_{S \rightarrow T}, D_T)$ is achieved if and only if $p_t(x, y) = p_g(x, y) = p_c(x, y)$, where $\tilde{\mathcal{L}}$ is defined as*

$$\tilde{\mathcal{L}}(C, G_{S \rightarrow T}, D_T) = \mathcal{L}_{GAN} + \mathcal{L}_C + \mathcal{L}_{cycle}.$$

Practical Convergence. Despite the theoretical proof of the Nash equilibrium, it is insufficient to guarantee our model achieving such equilibrium under the practical optimization with stochastic gradient descent [29, 2, 11]. Therefore, we adopt a tool called Path Angle [3] to verify the effectiveness of our model’s practical convergence property.

In practice, studying the game vector field (i.e., the concatenation of both networks’ gradient) around the local stable stationary point (LSSP), which is a necessary condition for Nash equilibrium, is an alternative point of view that can provide better insights of the practical convergence [29, 10]. Compared to Nash equilibrium which corresponds to the static stability, LSSP captures the dynamic stability of the training process. Path Angle provides insights about the convergence property around the LSSP. To calculate it, we first linearly interpolate models between the initial parameters and the final parameters, then compute gradients for these models. The convergence characteristic around the LSSP can be analyzed by (1) the gradient norm and (2) the angle between the gradient vector and the interpolation line. We refer readers to the original paper for more details.

As shown in Fig. 4(a), relaxed cGAN shows a change of direction and smaller gradient norm when the training is close to the convergence (represented as point 1.0 of x-axis). Such a pattern shows an attraction field referring Fig. 4(c) where the gradient direction always points to the LSSP and the norm decreases as being close to it. The mode indicates that during training, relaxed cGAN can converge to a point that is close to LSSP and thus can get excellent performance.

For comparison, we also visualize the training dynamics of the preliminary cGAN framework introduced in Sec. 3. As shown in Fig. 4(b), the preliminary method always has the cosine value close to 0, showing rotation phenomena. Besides, the gradient norm is relatively large and continues to decrease, which means that the preliminary method is still far from the LSSP but the model cannot reach there because of rotation. Such poor practical convergence property

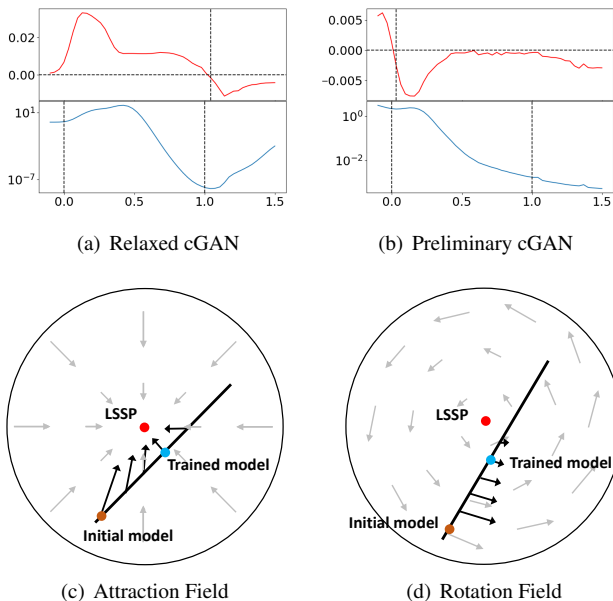


Figure 4: Visualization of the practical convergence of Relaxed cGAN and Preliminary cGAN. (a) and (b) visualize their vector field statistics. The upper red line is the cosine angle between the gradient vector and the interpolation path. The lower blue line is the corresponding gradient norm. The X-axis means the interpolation point. (c) and (d) are the game vector field imitated for Relaxed cGAN and Preliminary cGAN respectively. Black arrows show the gradient direction at different linear interpolations between the initial model and the final trained model. The gradients of Relaxed cGAN point to the LSSP while in Preliminary cGAN they are perpendicular to the interpolation line. It shows that Relaxed cGAN performs better than the Preliminary cGAN under practical training.

may offer a possible explanation of why even though the preliminary method have the same Nash equilibrium as Relaxed cGAN does [12], it encounters the label-domination problem and gives poor results for classification — the model always outputs different prototypes during training just like rotation but cannot converge to an LSSP.

Image Transfer Results. We further validate our design in terms of image transformation. As shown in Fig. 5, the generated samples are of high quality.

4.3. Additional Regularization

Apart from the label-domination problem, it is crucial to leverage the large amount of unlabeled data in the target domain to improve the results in SSDA. To this end, we add a marginal loss such that the discriminator accepts all the real images in the target domain (including labeled data and

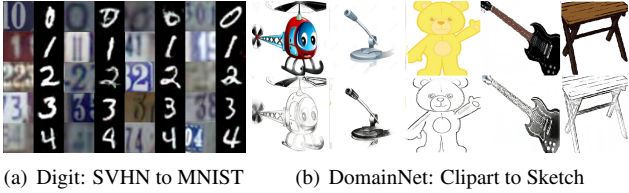


Figure 5: The generation results of Relaxed cGAN. For the digit experiment, the odd column is the input image and the even column is the generated image. For DomainNet experiment, the upper row is the input image and the lower row is the generated image. As we can see, the generated images are of high quality and their labels follow the ground truth of input labels.

unlabeled data). In particular, we feed an extra $(K + 1)$ -th class to the discriminator (same discriminator as before), where K is the number of classes of the data. All the target images belong to the $(K + 1)$ -th class. The marginal loss function for D is defined as:

$$\begin{aligned} \mathcal{L}_{margin} = & \mathbb{E}_{x \sim p_t(x)} [\log(D_T(x, K + 1))] \\ & + \mathbb{E}_{x \sim p_u(x)} [\log(D_T(x, K + 1))] \\ & + \mathbb{E}_{x \sim p_s(x)} [\log(1 - D_T(G_{S \rightarrow T}(x), K + 1))], \end{aligned}$$

The first two items are positive samples for the discriminator from the labeled and unlabeled target data. The third item represents the negative samples as they come from the generator.

Intuitively, the marginal loss can avoid that the discriminator only memorizes the empirical distribution of labeled data. Further, we prove that the marginal loss would not change the equilibrium of the three networks (see Appendix A for more details), and we verify the effectiveness of the marginal loss in both image classification (see Table. 5) and image transfer (see Appendix D).

Therefore, the overall loss function would be

$$\mathcal{L} = \lambda_{GAN} \mathcal{L}_{GAN} + \lambda_{cycle} \mathcal{L}_{cycle} + \lambda_C \mathcal{L}_C + \lambda_{margin} \mathcal{L}_{margin}.$$

5. Experiments

5.1. Setup

We first evaluate the proposed Relaxed cGAN in two practical SSDA settings on Digit adaptation benchmarks, including (1) **High-resource SSDA**, where we have full access to the target dataset’s unlabeled data and a few labeled data. (2) **Low-resource SSDA**, where the number of unlabeled data in the target domain is also limited. Secondly, we verify our approach on several large-scale image datasets, namely, DomainNet [36] and Office-Home[44].

Datasets. We first perform experiments on three benchmark **Digit** datasets, including MNIST [23], USPS [8]

and SVHN [34], all of which are 10-class classification tasks. Both MNIST and USPS are datasets consisting of grayscale images of handwritten digits. SVHN is a more diverse house number dataset which is obtained by cropping Google Street View images. For **DomainNet**, we follow the experiment settings of [39] and choose 4 domains: Real(R), Clipart(C), Sketch(S) and Painting(P), with 126 shared classes across domains. **Office-Home** is another standard benchmark for domain adaptation, containing 4 domains (Real, Clipart, Art, and Product).

Implementation Details. (1) **Preprocessing.** All images are normalized with a mean of 0.5 and a standard deviation of 0.5. For digit tasks, images are resized to 32×32 . We duplicate MNIST and USPS image channels 3 times to match the channel size of SVHN. For DomainNet, images are resized to 256×256 , according to our design of the generator. (2) **Network Details.** For adaptation between USPS and MNIST, we employ a simple architecture. For transfer tasks from SVHN to MNIST and SVHN to USPS, we adopt a slightly complex architecture. For DomainNet, we use imagenet-pretrained Alexnet [22] as the classifier. The base architecture of the generator and the discriminator mainly follows the default design of cycleGAN, except conditional input and Spectral Normalization. See more details in Appendix B. (3) **Training Techniques.** To further make use of unlabeled data, we apply widely adopted entropy minimization loss [13] denoted as \mathcal{L}_{ENT} . For DomainNet and Office-Home, we adopt source data supervision as a regularization. To avoid that the discriminator overfits on labeled images, we generate pseudo labels using the classifier C for randomly selected unlabeled images and feed the image-label pairs as positive samples to D_T for training. Corresponding loss is defined as follows:

$$\mathcal{L}_{pseudo} = \mathbb{E}_{x \sim p_u(x)} [\log(D_T(x, C(x)))].$$

Note that this loss performs conversely against the third item in Eqn. (2) which may introduce some biases to the target distribution, resulting in a mixture distribution of p_c and p_t . However, since p_c and p_t are close, such bias may be neglected in practice.

Baselines. We mainly divide our baselines into two categories: feature-level and pixel-level adaptation. (1) **Digit High-resource SSDA.** We compare our proposed method with two feature-level methods, F-CADA [46] and AVDA [37]. Since few pixel-level methods explore the setting of SSDA, we compare with CyCADA [16] and ACAL [17] which are strong methods proposed for Un-supervised Domain Adaptation(UDA) and Supervised Domain Adaptation(SDA) respectively. For a fair comparison, We extend their methods by adding the supervised loss \mathcal{L}_C

dataset	# of label	pixel-level				feature-level	
		Relaxed cGAN	cycleGAN [45] + \mathcal{L}_C + \mathcal{L}_{ENT}	CyCADA [16] + \mathcal{L}_C	ACAL [17] + \mathcal{L}_{ENT}	AVDA [37]	F-CADA [46] (best)
$\mathcal{S} \rightarrow \mathcal{M}$	1	95.9±2.8	70.2±6.8	90.6±0.1	80.5±0.8	95.1±0.5	94.8
	2	96.3±1.3	81.3±3.0	90.8±0.3	94.9±0.9	-	95.1
	3	96.9±0.4	81.7±3.9	90.8±0.5	94.5±0.3	-	95.4
	4	97.0±0.4	83.3±2.9	90.7±0.2	94.8±0.5	-	95.5
	5	97.5±0.3	84.5±3.6	90.6±0.6	94.9±0.6	96.9±0.2	95.6
	6	98.0±0.5	86.4±2.4	91.5±0.3	96.0±0.9	-	95.9
	7	98.0±0.5	85.3±2.9	91.3±0.2	96.3±0.7	-	96.1
$\mathcal{U} \rightarrow \mathcal{M}$	1	98.7±0.6	78.7±0.9	96.0±0.3	81.3±9.3	98.3±0.3	97.5
	2	99.0±0.2	82.4±4.0	96.2±0.2	93.2±2.9	-	97.8
	3	99.0±0.2	86.3±5.1	96.1±0.1	89.2±6.8	-	98.1
	4	99.1±0.1	82.5±2.3	96.5±0.1	92.4±3.9	-	98.4
	5	99.1±0.1	83.9±3.5	96.3±0.2	94.4±1.1	98.6±0.03	98.6
	6	99.2±0.1	84.5±3.9	96.5±0.2	95.3±0.8	-	98.8
	7	99.2±0.1	82.9±2.9	96.3±0.2	95.6±0.6	-	98.9
$\mathcal{M} \rightarrow \mathcal{U}$	1	97.9±0.5	81.7±1.3	94.2±0.4	68.3±12.9	98.4±0.3	97.2
	2	98.0±0.2	84.7±2.2	94.0±0.3	86.1±2.9	-	97.5
	3	98.0±0.3	85.0±4.7	94.4±0.4	82.0±1.6	-	97.9
	4	98.2±0.3	81.4±3.1	95.0±0.3	84.8±8.7	-	98.1
	5	98.2±0.1	85.5±1.2	95.0±0.1	88.2±2.7	98.5±0.2	98.3
	6	98.4±0.1	86.4±5.2	94.5±0.5	83.0±1.6	-	98.4
	7	98.2±0.1	82.9±3.2	95.1±0.2	90.2±2.7	-	98.6

Table 1: Digit High-resource SSDA. CyCADA [16] and ACAL [17] are two pixel-level methods proposed for Unsupervised Domain Adaptation and Supervised Domain Adaptation respectively. We extend their method for SSDA by adding the supervised loss \mathcal{L}_C and the semi-supervised loss \mathcal{L}_{ENT} for a fair comparison. AVDA [37] and F-CADA [46] are two feature-level methods. All experiments are performed 3 times and we report both the average accuracy and standard deviation. Our method outperforms all baselines on $\mathcal{S} \rightarrow \mathcal{M}$ and $\mathcal{U} \rightarrow \mathcal{M}$, and achieve comparable results on $\mathcal{M} \rightarrow \mathcal{U}$.

	$\mathcal{S} \rightarrow \mathcal{M}$			$\mathcal{M} \rightarrow \mathcal{U}$			$\mathcal{U} \rightarrow \mathcal{M}$			$\mathcal{S} \rightarrow \mathcal{U}$			
	# of labels per class	5	10	600	5	10	72	5	10	600	5	10	72
# of data per class	50	100	6000	50	100	729	50	100	6000	50	100	729	
cycleGAN [45]	68.3	81.3	96.0	94.5	95.8	95.9	92.4	92.8	97.0	66.7	77.5	90.6	
ACAL [17]	87.2	91.8	99.4	94.2	96.0	95.7	96.8	96.9	98.5	86.2	89.0	93.2	
Relaxed cGAN	96.9	97.7	99.6	97.1	97.5	98.1	96.9	97.1	99.6	94.6	96.4	98.2	

Table 2: Digit Low-resource SSDA. We follow the settings of the pixel-level method ACAL where unlabeled data in the target domain are also limited. Relaxed cGAN achieves SOTA in all settings.

and the semi-supervised loss \mathcal{L}_{ENT} , respectively. **(2) Digit Low-resource SSDA.** It is an important setting proposed by ACAL [17] that few unlabeled data on the target domain are available. We also compare our model with their method. The results of cycleGAN are also listed for reference. **(3) DomainNet & Office-Home.** MME [39], MetaMME [25] and APE [21] are 3 feature-level methods. A recent work called BiAT [19] generates images by adversarial training, so we choose their work as our pixel-level baseline.

5.2. Results

Digit High-resource SSDA. In the Digit high-resource SSDA settings, we could access the whole training dataset of the target domain with partially labeled data. We adopt the same experimental settings as in F-CADA [46] and

AVDA [37], where the number of the labeled data in each class is set from 1 to 7. Following AVDA [37], we report both the averaged accuracy (with the standard deviation) over three runs as well as the best of them. As shown in Table 1, both the average and the best results of Relaxed cGAN consistently outperform the SSDA baselines under $\mathcal{S} \rightarrow \mathcal{M}$ and $\mathcal{U} \rightarrow \mathcal{M}$, suggesting that Relaxed cGAN performs effective adaptation.

In $\mathcal{M} \rightarrow \mathcal{U}$, the number of unlabeled data is about ten percent of that in the former two settings, making the adaptation process harder. Nevertheless, Relaxed cGAN still achieves the best performance in five out of the seven settings and is competitive with the strong feature-level baselines in the other two settings.

Digit Low-resource SSDA. In the low-resource SSDA

	Relaxed cGAN	BiAT [19]	APE [21]	meta- MME [25]	MME [39]	ENT [13]	S+T
R to C	56.8	58.6	54.6	56.4	55.6	45.5	47.1
R to P	51.8	50.6	50.5	50.2	49.0	42.6	45.0
P to C	52.0	52.0	52.1	51.9	51.7	40.4	44.9
C to S	44.1	41.9	42.6	39.6	39.4	31.1	36.4
S to P	44.2	42.1	42.2	43.7	43.0	29.6	38.4
R to S	42.8	42.0	38.7	38.7	37.9	29.6	33.3
P to R	61.1	58.8	61.4	60.7	60.7	60.0	58.7
AVG	50.5	49.4	48.9	48.8	48.2	39.8	43.4

Table 3: DomainNet results. All experiments are conducted under the 3-shot setting with an Alexnet backbone. Our method outperforms baselines in most settings and achieves SOTA on the average results.

settings, the number of unlabeled data in the target domain is also limited. We compare against the representative pixel-level baselines cycleGAN [45] and ACAL [17], following the same experiment settings in ACAL for fairness. The number of available images in the target domain is set to 50, 100, and full per class, and the labeled samples take 10% of the available target samples. We present the experiment results in Table 2. It can be seen that our method significantly outperforms cycleGAN and ACAL in all settings even though we do not apply any form of semantic consistency loss as mentioned in ACAL. This mainly benefits from our solution to both label-inconsistency and label-domination problem. Besides, we show that the images generated from Relaxed cGAN are of correct semantics and higher quality, compared to those from the baselines in Fig. 1 and Appendix D. Such results agree with the classification performance and well support our motivation.

DomainNet & Office-Home. We further evaluate Relaxed cGAN on two large-scale image datasets, DomainNet and Office-Home. We conduct all experiments under the 3-shot setting with a pretrained Alexnet backbone. We choose the label data in the target domain following the setting of [39].

As shown in Table 3, on DomainNet our method surpasses ENT [13] by a large margin, which uses the same loss function as the classifier in Relaxed cGAN. This suggests that thanks to the carefully designed generator and discriminator, the transferred images can provide useful learning signals to the classifier. Further, as a pixel-level method, Relaxed cGAN achieves SOTA results on DomainNet demonstrating its scalability on large datasets. Similar results are obtained on Office-Home referring to Table 4, where Relaxed cGAN outperforms existing powerful methods.

5.3. Ablation Study

We conduct several quantitative ablation studies to analyze the contribution of each component on digit bench-

	Relaxed cGAN	APE [21]	meta- MME [25]	MME [39]	ENT [13]	S+T
R to C	68.4	66.4	65.2	64.6	62.6	55.7
R to P	85.5	86.2	-	85.5	85.7	80.8
R to A	73.8	73.4	-	71.3	70.2	67.8
P to R	81.2	82.0	-	80.1	79.9	73.1
P to C	68.1	65.2	64.5	64.6	60.5	53.8
P to A	67.9	66.1	66.7	65.5	63.9	63.5
A to P	79.0	81.1	-	79.0	79.5	73.1
A to C	64.3	63.9	63.3	63.6	61.3	54.0
A to R	80.1	80.2	-	79.7	79.1	74.2
C to R	77.5	76.8	-	76.6	76.4	68.3
C to A	66.3	66.6	67.5	67.2	64.7	57.6
C to P	78.3	79.9	-	79.3	79.1	72.3
AVG	74.2	74.0	-	73.1	71.9	66.2

Table 4: Office-Home results under 3-shot setting with an ResNet-34 backbone. Relaxed cGAN outperforms baselines in most settings and achieves SOTA on the average results.

	$\mathcal{S} \rightarrow \mathcal{M}$	$\mathcal{M} \rightarrow \mathcal{U}$	$\mathcal{U} \rightarrow \mathcal{M}$
ENT	83.9	85.1	83.9
cycleGAN	68.4	95.9	94.2
Preliminary Method	87.8	82.1	84.9
Relaxed cGAN w/o. $\mathcal{L}_{margin}, \mathcal{L}_{pseudo}$	94.3	96.4	96.2
Relaxed cGAN	95.9	97.9	98.7

Table 5: Ablation Study. We conduct all the experiments under the 1-shot setting on 3 adaptation tasks. **ENT**: semi-supervised learning on both labeled and unlabeled target data with \mathcal{L}_{ENT} . **Relaxed cGAN w/o.** $\mathcal{L}_{margin}, \mathcal{L}_{pseudo}$: Relaxed cGAN without the \mathcal{L}_{margin} and \mathcal{L}_{pseudo} .

marks in the high-resource SSDA settings, with 1 annotated samples for each class. The results are shown in Table 5.

Label-inconsistency and Label-domination. As shown in Table 5, cycleGAN encounters label-inconsistency problem when the domain shift is large ($\mathcal{S} \rightarrow \mathcal{M}$). The Preliminary Method encounters the label-domination problem and only shows comparable results as the entropy-minimization (ENT) on the target domain. The proposed Relaxed cGAN resolves both problems and surpasses the above two approaches by a large margin.

Additional Regularization. We show the effectiveness of both marginal loss and pseudo loss together as they all try to make better use of unlabeled data. As we can see from the last two rows of Table 5, these additional regularizations further boost Relaxed cGAN’s performance on SSDA.

6. Conclusion

In this work, we focus on the setting of SSDA. We identify the label-domination problem raised by the conditional GAN framework during the image transformation. We then

elaborately design Relaxed cGAN to resolve this issue. Its generator takes images as the only input, while its discriminator takes image-label pairs. By doing this, the generator has to infer the input data’s semantic information. The proposed model has a provable and satisfied theoretical equilibrium. Its practical convergence property and image transfer quality are also empirically shown to be effective. Extensive experimental results show that the proposed Relaxed cGAN achieves state-of-the-art results in DomainNet and several digit adaptation benchmarks under both low-resource and high-resource SSDA settings. The model also obtains competitive results in the Office-Home benchmark.

Acknowledgement

This work was supported by the National Key Research and Development Program of China (Nos. 2017YFA0700904, 2020AAA0104304), NSFC Projects (Nos. 61620106010, 62076145, U19B2034, U1811461, U19A2081), Beijing NSF Project (No. L172037), Beijing Academy of Artificial Intelligence (BAAI), THU-Bosch JCML center, Tsinghua-Huawei Joint Research Program, a grant from Tsinghua Institute for Guo Qiang, Tiangong Institute for Intelligent Computing, the JP Morgan Faculty Research Program and the NVIDIA NVAIL Program with GPU/DGX Acceleration. C. Li was supported by the Chinese postdoctoral innovative talent support program and Shuimu Tsinghua Scholar.

References

- [1] Martin Arjovsky, Soumith Chintala, and Léon Bottou. Wasserstein gan. *arXiv preprint arXiv:1701.07875*, 2017. **2**
- [2] David Balduzzi, Sebastien Racaniere, James Martens, Jakob Foerster, Karl Tuyls, and Thore Graepel. The mechanics of n-player differentiable games. *arXiv preprint arXiv:1802.05642*, 2018. **5**
- [3] Hugo Berard, Gauthier Gidel, Amjad Almahairi, Pascal Vincent, and Simon Lacoste-Julien. A closer look at the optimization landscapes of generative adversarial networks. *arXiv preprint arXiv:1906.04848*, 2019. **5**
- [4] Bharath Bhushan Damodaran, Benjamin Kellenberger, Rémi Flamary, Devis Tuia, and Nicolas Courty. Deepjdot: Deep joint distribution optimal transport for unsupervised domain adaptation. In *Proceedings of the European Conference on Computer Vision (ECCV)*, pages 447–463, 2018. **1**
- [5] Konstantinos Bousmalis, Nathan Silberman, David Dohan, Dumitru Erhan, and Dilip Krishnan. Unsupervised pixel-level domain adaptation with generative adversarial networks. In *Proceedings of the IEEE Conference on Computer Vision and Pattern Recognition*, pages 3722–3731, 2017. **1, 2**
- [6] Debasmrit Das and CS George Lee. Graph matching and pseudo-label guided deep unsupervised domain adaptation. In *International Conference on Artificial Neural Networks*, pages 342–352. Springer, 2018. **2**
- [7] Weijian Deng, Liang Zheng, Qixiang Ye, Guoliang Kang, Yi Yang, and Jianbin Jiao. Image-image domain adaptation with preserved self-similarity and domain-dissimilarity for person re-identification. In *Proceedings of the IEEE Conference on Computer Vision and Pattern Recognition*, pages 994–1003, 2018. **2**
- [8] John S Denker, WR Gardner, Hans Peter Graf, Donnie Henderson, Richard E Howard, W Hubbard, Lawrence D Jackel, Henry S Baird, and Isabelle Guyon. Neural network recognizer for hand-written zip code digits. In *Advances in Neural Information Processing Systems*, pages 323–331, 1989. **6**
- [9] Yaroslav Ganin, Evgeniya Ustinova, Hana Ajakan, Pascal Germain, Hugo Larochelle, François Laviolette, Mario Marchand, and Victor Lempitsky. Domain-adversarial training of neural networks. *The Journal of Machine Learning Research*, 17(1):2096–2030, 2016. **1, 2**
- [10] Gauthier Gidel, Hugo Berard, Gaëtan Vignoud, Pascal Vincent, and Simon Lacoste-Julien. A variational inequality perspective on generative adversarial networks. *arXiv preprint arXiv:1802.10551*, 2018. **5**
- [11] Gauthier Gidel, Reyhane Askari Hemmat, Mohammad Pezeshki, Rémi Le Priol, Gabriel Huang, Simon Lacoste-Julien, and Ioannis Mitliagkas. Negative momentum for improved game dynamics. In *The 22nd International Conference on Artificial Intelligence and Statistics*, pages 1802–1811, 2019. **5**
- [12] Ian Goodfellow, Jean Pouget-Abadie, Mehdi Mirza, Bing Xu, David Warde-Farley, Sherjil Ozair, Aaron Courville, and Yoshua Bengio. Generative adversarial nets. In *Advances in Neural Information Processing Systems*, pages 2672–2680, 2014. **4, 5**
- [13] Yves Grandvalet and Yoshua Bengio. Semi-supervised learning by entropy minimization. In *Advances in Neural Information Processing Systems*, pages 529–536, 2005. **6, 8**
- [14] Arthur Gretton, Karsten Borgwardt, Malte Rasch, Bernhard Schölkopf, and Alex J Smola. A kernel method for the two-sample-problem. In *Advances in Neural Information Processing Systems*, pages 513–520, 2007. **2**
- [15] Kaiming He, Xiangyu Zhang, Shaoqing Ren, and Jian Sun. Deep residual learning for image recognition. In *Proceedings of the IEEE Conference on Computer Vision and Pattern Recognition*, pages 770–778, 2016. **1**
- [16] Judy Hoffman, Eric Tzeng, Taesung Park, Jun-Yan Zhu, Phillip Isola, Kate Saenko, Alexei A Efros, and Trevor Darrell. Cycada: Cycle-consistent adversarial domain adaptation. *arXiv preprint arXiv:1711.03213*, 2017. **1, 2, 6, 7**
- [17] Ehsan Hosseini-Asl, Yingbo Zhou, Caiming Xiong, and Richard Socher. Augmented cyclic adversarial learning for domain adaptation. *arXiv preprint arXiv:1807.00374*, 1(3), 2018. **1, 2, 6, 7, 8**
- [18] Sheng-Wei Huang, Che-Tsung Lin, Shu-Ping Chen, Yen-Yi Wu, Po-Hao Hsu, and Shang-Hong Lai. Auggan: Cross domain adaptation with gan-based data augmentation. In *Proceedings of the European Conference on Computer Vision (ECCV)*, pages 718–731, 2018. **1**

- [19] Pin Jiang, Aming Wu, Yahong Han, Yunfeng Shao, Meiyu Qi, and Bingshuai Li. Bidirectional adversarial training for semi-supervised domain adaptation. **7, 8**
- [20] Guoliang Kang, Lu Jiang, Yi Yang, and Alexander G Hauptmann. Contrastive adaptation network for unsupervised domain adaptation. In *Proceedings of the IEEE Conference on Computer Vision and Pattern Recognition*, pages 4893–4902, 2019. **1**
- [21] Taekyung Kim and Changick Kim. Attract, perturb, and explore: Learning a feature alignment network for semi-supervised domain adaptation. *arXiv preprint arXiv:2007.09375*, 2020. **7, 8**
- [22] Alex Krizhevsky, Ilya Sutskever, and Geoffrey E Hinton. Imagenet classification with deep convolutional neural networks. In *Advances in Neural Information Processing Systems*, pages 1097–1105, 2012. **1, 6**
- [23] Yann LeCun, Léon Bottou, Yoshua Bengio, and Patrick Haffner. Gradient-based learning applied to document recognition. *Proceedings of the IEEE*, 86(11):2278–2324, 1998. **2, 6**
- [24] Chongxuan Li, Taufik Xu, Jun Zhu, and Bo Zhang. Triple generative adversarial nets. In *Advances in Neural Information Processing Systems*, pages 4088–4098, 2017. **4**
- [25] Da Li and Timothy Hospedales. Online meta-learning for multi-source and semi-supervised domain adaptation. *arXiv preprint arXiv:2004.04398*, 2020. **7, 8**
- [26] Ming-Yu Liu, Thomas Breuel, and Jan Kautz. Unsupervised image-to-image translation networks. In *Advances in neural information processing systems*, pages 700–708, 2017. **1**
- [27] Mingsheng Long, Han Zhu, Jianmin Wang, and Michael I Jordan. Deep transfer learning with joint adaptation networks. In *Proceedings of International Conference on Machine Learning*, pages 2208–2217. JMLR. org, 2017. **1, 2**
- [28] Yawei Luo, Liang Zheng, Tao Guan, Junqing Yu, and Yi Yang. Taking a closer look at domain shift: Category-level adversaries for semantics consistent domain adaptation. In *Proceedings of the IEEE Conference on Computer Vision and Pattern Recognition*, pages 2507–2516, 2019. **1**
- [29] Lars Mescheder, Sebastian Nowozin, and Andreas Geiger. The numerics of gans. In *Advances in Neural Information Processing Systems*, pages 1825–1835, 2017. **5**
- [30] Mehdi Mirza and Simon Osindero. Conditional generative adversarial nets. *arXiv preprint arXiv:1411.1784*, 2014. **2, 3**
- [31] Saeid Motiian, Quinn Jones, Seyed Iranmanesh, and Gianfranco Doretto. Few-shot adversarial domain adaptation. In *Advances in Neural Information Processing Systems*, pages 6670–6680, 2017. **1, 2**
- [32] Saeid Motiian, Marco Piccirilli, Donald A Adjeroh, and Gianfranco Doretto. Unified deep supervised domain adaptation and generalization. In *Proceedings of the IEEE International Conference on Computer Vision*, pages 5715–5725, 2017. **2**
- [33] Zak Murez, Soheil Kolouri, David Kriegman, Ravi Ramamoorthi, and Kyungnam Kim. Image to image translation for domain adaptation. In *Proceedings of the IEEE Conference on Computer Vision and Pattern Recognition*, pages 4500–4509, 2018. **1, 2**
- [34] Yuval Netzer, Tao Wang, Adam Coates, Alessandro Bisaccho, Bo Wu, and Andrew Y Ng. Reading digits in natural images with unsupervised feature learning. 2011. **2, 6**
- [35] Sinno Jialin Pan and Qiang Yang. A survey on transfer learning. *IEEE Transactions on Knowledge and Data Engineering*, 22(10):1345–1359, 2009. **1**
- [36] Xingchao Peng, Qinxun Bai, Xide Xia, Zijun Huang, Kate Saenko, and Bo Wang. Moment matching for multi-source domain adaptation. In *Proceedings of the IEEE International Conference on Computer Vision*, pages 1406–1415, 2019. **6**
- [37] Manuel Pérez-Carrasco, Guillermo Cabrera-Vives, Pavlos Protopapas, Nicolás Astorga, and Marouan Belhaj. Matching embeddings for domain adaptation. *arXiv*, pages arXiv–1909, 2019. **1, 2, 6, 7**
- [38] Artem Rozantsev, Mathieu Salzmann, and Pascal Fua. Beyond sharing weights for deep domain adaptation. *IEEE Transactions on Pattern Analysis and Machine Intelligence*, 41(4):801–814, 2018. **2**
- [39] Kuniaki Saito, Donghyun Kim, Stan Sclaroff, Trevor Darrell, and Kate Saenko. Semi-supervised domain adaptation via minimax entropy. In *Proceedings of the IEEE International Conference on Computer Vision*, pages 8050–8058, 2019. **1, 2, 6, 7, 8**
- [40] Kuniaki Saito, Kohei Watanabe, Yoshitaka Ushiku, and Tatsuya Harada. Maximum classifier discrepancy for unsupervised domain adaptation. In *Proceedings of the IEEE Conference on Computer Vision and Pattern Recognition*, pages 3723–3732, 2018. **1**
- [41] Christian Szegedy, Wei Liu, Yangqing Jia, Pierre Sermanet, Scott Reed, Dragomir Anguelov, Dumitru Erhan, Vincent Vanhoucke, and Andrew Rabinovich. Going deeper with convolutions. In *Proceedings of the IEEE Conference on Computer Vision and Pattern Recognition*, pages 1–9, 2015. **1**
- [42] Hui Tang, Ke Chen, and Kui Jia. Unsupervised domain adaptation via structurally regularized deep clustering. In *Proceedings of the IEEE/CVF Conference on Computer Vision and Pattern Recognition*, pages 8725–8735, 2020. **1**
- [43] Eric Tzeng, Judy Hoffman, Kate Saenko, and Trevor Darrell. Adversarial discriminative domain adaptation. In *Proceedings of the IEEE Conference on Computer Vision and Pattern Recognition*, pages 7167–7176, 2017. **1, 2**
- [44] Hemanth Venkateswara, Jose Eusebio, Shayok Chakraborty, and Sethuraman Panchanathan. Deep hashing network for unsupervised domain adaptation. In *Proceedings of the IEEE Conference on Computer Vision and Pattern Recognition*, pages 5018–5027, 2017. **6**
- [45] Jun-Yan Zhu, Taesung Park, Phillip Isola, and Alexei A Efros. Unpaired image-to-image translation using cycle-consistent adversarial networks. In *Proceedings of the IEEE international conference on computer vision*, pages 2223–2232, 2017. **1, 2, 7, 8**
- [46] Han Zou, Yuxun Zhou, Jianfei Yang, Huihan Liu, Hari Prasanna Das, and Costas J Spanos. Consensus adversarial domain adaptation. In *Proceedings of the AAAI Conference on Artificial Intelligence*, volume 33, pages 5997–6004, 2019. **1, 2, 6, 7**

Supplementary Material for "Relaxed Conditional Image Transfer for Semi-supervised Domain Adaptation"

1 Appendix A: Equilibrium Analysis

For the ease of the proof, we define our objective function for the game of three networks C , $G_{S \rightarrow T}$ and D_T as:

$$\min_{C, G_{S \rightarrow T}} \max_{D_T} \tilde{U}(C, G_{S \rightarrow T}, D_T) = \min_{C, G_{S \rightarrow T}} \max_{D_T} \mathcal{L}_{GAN}(C, G_{S \rightarrow T}, D_T) + \min_C \mathcal{L}_C, \quad (1)$$

where

$$\begin{aligned} \mathcal{L}_{GAN}(C, G_{S \rightarrow T}, D_T) &= \mathbb{E}_{(x,y) \sim p_t(x,y)} [\log(D_T(x, y))] \\ &\quad + \alpha \mathbb{E}_{(x,y) \sim p_s(x,y)} [\log(1 - D_T(G_{S \rightarrow T}(x), y))] \\ &\quad + ((1 - \alpha) \mathbb{E}_{(x,y) \sim p_s(x,y)} [\log(1 - D_T(x, C(x)))]), \end{aligned} \quad (2)$$

refer to \mathcal{L}_{GAN} and \mathcal{L}_C in Sec.4.

We first give the proof that the equilibrium of $\tilde{U}(C, G_{S \rightarrow T}, D_T)$ is achieved only when $p_t(x, y) = p_g(x, y) = p_c(x, y)$, under the nonparametric assumption [1]. After that, a corollary is shown that adding other losses, such as L_{cycle} , L_{marg} , L_{ent} , will not change such equilibrium of our framework.

Lemma 1.1. *For any fixed C and $G_{S \rightarrow T}$, the optimal discriminator D_T of the game defined by the objective function $U(C, G_{S \rightarrow T}, D_T)$ is*

$$D_{T|C, G_{S \rightarrow T}}^*(x, y) = \frac{p_t(x, y)}{p_t(x, y) + p_m(x, y)}, \quad (3)$$

where $p_m(x, y) := \alpha p_g(x, y) + (1 - \alpha) p_c(x, y)$ is a mixture distribution of $p_g(x, y)$ and $p_c(x, y)$.

Proof. Given the classifier and generator, the objective function can be rewritten as

$$\begin{aligned} U(C, G_{S \rightarrow T}, D_T) &= \iint p_t(x, y) \log D_T(x, y) dy dx \\ &\quad + \alpha \iint p(y) p_s(x) \log(1 - D_T(G_{S \rightarrow T}(x), y)) dy dx \\ &\quad + (1 - \alpha) \iint p_t(x) p_c(y|x) \log(1 - D_T(x, y)) dy dx \\ &= \iint p_t(x, y) \log D_T(x, y) dy dx \\ &\quad + \iint p_m(x, y) \log(1 - D_T(x, y)) dy dx, \end{aligned}$$

which achieves the maximum at $\frac{p_t(x, y)}{p_t(x, y) + p_m(x, y)}$.

□

Given $D_{T|C, G_{S \rightarrow T}}^*$, we can reformulate the minimax game with value function V as:

$$V(C, G_{S \rightarrow T}) = \iint p_t(x, y) \log \frac{p_t(x, y)}{p_t(x, y) + p_m(x, y)} dy dx \\ + \iint p_m(x, y) \log \frac{p_m(x, y)}{p_t(x, y) + p_m(x, y)} dy dx.$$

Lemma 1.2. *The global minimum of $V(C, G_{S \rightarrow T})$ is achieved if and only if $p_t(x, y) = p_m(x, y)$.*

Proof. Following the proof in GAN [1], the $V(C, G_{S \rightarrow T})$ can be rewritten as

$$V(C, G_{S \rightarrow T}) = -\log 4 + 2\mathbb{D}_{JS}(p_t(x, y) || p_m(x, y)), \quad (4)$$

where \mathbb{D}_{JS} is the Jensen-Shannon divergence, which is always non-negative and the unique optimum is achieved if and only if $p_t(x, y) = p_m(x, y)$. \square

Theorem 1.3. *The equilibrium of $\tilde{U}(C, G_{S \rightarrow T}, D_T)$ is achieved if and only if $p_t(x, y) = p_g(x, y) = p_c(x, y)$.*

Proof. According to the definition, we have $\tilde{U}(C, G_{S \rightarrow T}, D_T) = \mathcal{L}_{GAN}(C, G_{S \rightarrow T}, D_T) + \mathcal{L}_C$. We can rewrite \mathcal{L}_C as:

$$\mathcal{L}_C = \mathbb{E}_{p_t(x, y)} [-\log p_c(y|x)] \\ = \mathbb{E}_{p_t(x, y)} [\log \frac{p_t(x, y)}{p_c(x, y)}] - \mathbb{E}_{p_t(x, y)} [\log p(y|x)] \\ = \mathcal{D}(p_t(x, y) || p_c(x, y)) + \mathbb{E}_{p_t(x)} [\mathcal{H}[p(y|x)]],$$

where $\mathcal{D}(\cdot || \cdot)$ denotes the KL-divergence and $\mathcal{H}[\cdot]$ denotes the differential entropy. Since the second term is a constant and determined by the data distribution, minimizing \mathcal{L}_C is equivalent to minimizing $\mathcal{D}(p_t(x, y) || p_c(x, y))$, which is always non-negative and zero if and only if $p_t(x, y) = p_c(x, y)$. Besides, the previous lemmas can also be applied to $\tilde{U}(C, G_{S \rightarrow T}, D_T)$, which indicates that $p_t(x, y) = p_m(x, y)$ at the global equilibrium and concludes the proof. \square

Corollary 1.3.1. *Adding any divergence (e.g. the KL divergence) between any two of the joint distributions or the conditional distributions or the marginal distributions to \tilde{U} as an additional regularization to be minimized, will not change the global equilibrium of \tilde{U} .*

Proof. This conclusion can be straightforwardly obtained by the global equilibrium point of \tilde{U} and the definition of a statistical divergence between two distributions. \square

2 Appendix B: Network Architecture

Since the digit dataset SVHN(\mathcal{S}) is more complex than MNIST(\mathcal{M}) and USPS(\mathcal{U}). We employ different architectures when transferring between the datasets including \mathcal{S} or not. For adaptation between \mathcal{U} and \mathcal{M} , a simple architecture is utilized, refer to the Simple G and Simple D in Fig. 1. The Complex G and Complex D of Fig. 1 are adopted in the transfer tasks from \mathcal{S} to \mathcal{M} and \mathcal{S} to \mathcal{U} . For DomainNet [6], we set the default setting of cycleGAN [8] as our base architecture, with modification of Spectral Normalization and the suitable hinge loss [5]. Alexnet [4] is our classifier following the setting of MME [7]. We implement the conditional discriminator by outputting a (K+1)-dim vector of which each entry is the logit of the corresponding class. K is the number of classes, and the class K+1 refers to the marginal loss, as discussed in Sec.3.1.

3 Appendix C: Label Domination Study

We conduct a series of experiments to demonstrate the existence of the label-domination problem. The first two sets of experiments show how we identify such a problem. The latter three experiments indicate that such a problem still exists even when we employ cycle consistency loss [8], complex architecture, and Spectral Normalization [5] to the original model, which are normally considered

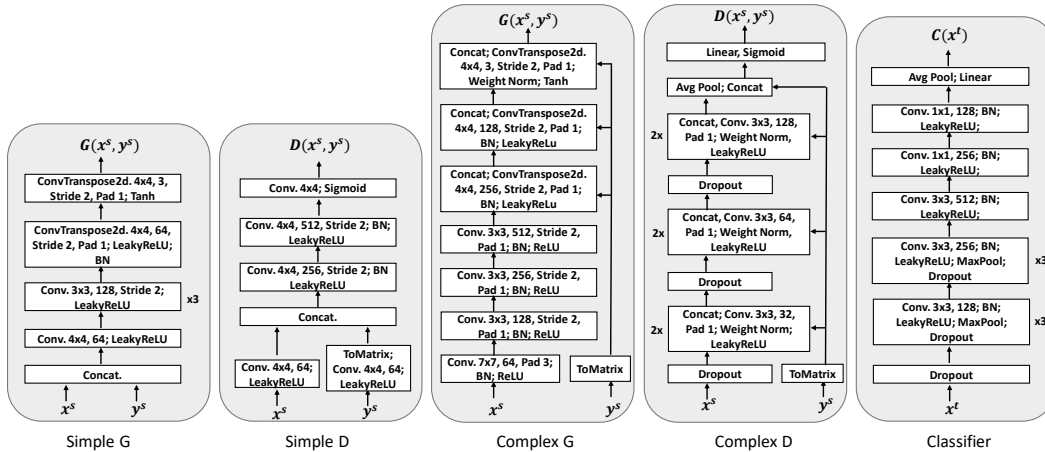


Figure 1: Network Architectures for digit datasets. "ToMatrix" means that each label is expanded to a $K * h * w$ feature map. The i -th channel is all set to 1, others are 0. K is the number of classes, i is the value of the label, h and w are the height and width of the image respectively.

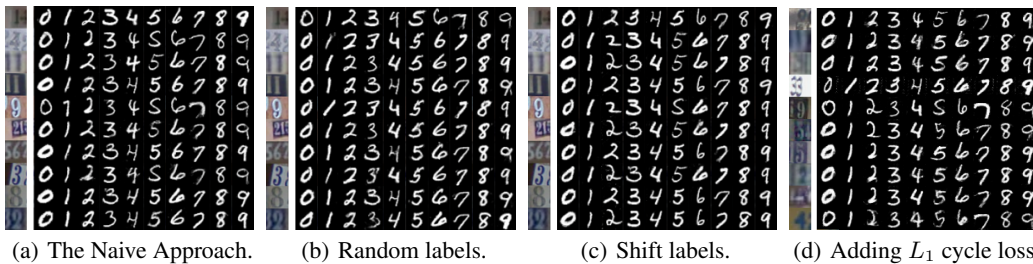


Figure 2: Label-domination problem. In each panel, the generator receives images from the leftmost column, paired with each label from '0' to '9'. In the right part, the image in the i -th row and j -th column is the corresponding generated image of the i -th input image and label ' j '. (a) The Naive Approach: the conditional generator and the conditional discriminator with correct image-label pairs are input to G during training stage. (b) Source images with random labels are input to G . (c) Source images with shift labels ('1' to '2', '2' to '3', and so on) as input to G . (d) The Naive Approach with cycle-consistency loss. The label-domination problem occurs in all settings.

as useful ways to solve the problem. All experiments are conducted in $\mathcal{S} \rightarrow \mathcal{M}$, following the description of Sec.3.2.

Inference with incorrect labels. We use the straight-forward approach with the conditional generator and the conditional discriminator described in Sec.3.2 for training. However, during inference, we feed source images with different labels to see if the information of the source images is taken into account during the transferring procedure. The results in Fig. 2 (a) show that the generated images completely follow the input label and ignore the source images' information.

Training with random and shifted labels. We further construct two validation approaches to better show that the source image is indeed be ignored during transfer. The generator is fed a source image with a random label or a label shifted by one (e.g., from '1' to '2' and '2' to '3' and so on) respectively in model training (namely, we input wrong image-label pairs to the generator). The discriminator still accepts the real label-data pairs in the target domain. Again, during inference, we feed source images with different labels, and the results are shown in Fig. 2 (b-c). We observe the same phenomenon of these two settings as the naive approach that the label-domination still holds. Besides, by adopting our jointly-training framework for SSDA, the accuracy of the Naive Approach, Random labels, and Shift labels are close to each other, with 88.0%, 87.9%, and 87.5% respectively. The generation and the accuracy indirectly show that the semantic information of the source image itself is ignored.

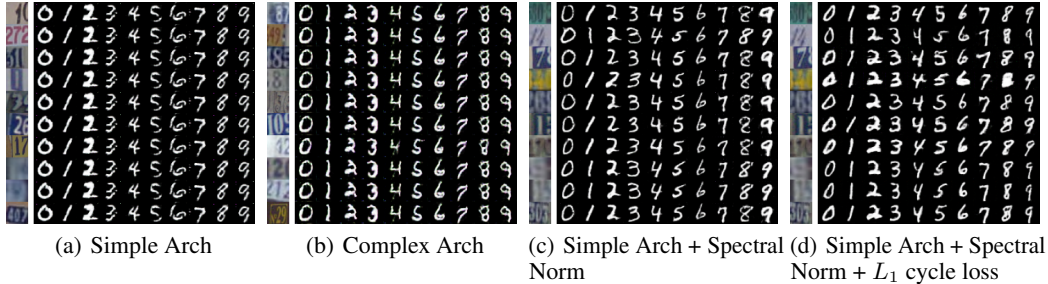


Figure 3: Label Domination Problem still occurs with a complex architecture, Spectral Normalization and cycle consistency loss.

Cycle Consistency Loss. Cycle-consistency loss is a widely adopted loss for maintaining the pixel-level correlation between the source image and the transferred image, which is proposed by [8]. We apply the cycle-consistency loss to the straight-forward approach to see if the label domination problem can be relieved. The results are presented in Fig. 3(d). As we can see, the label domination problem still exists.

Different Model Architectures. To eliminate the impact of model architecture, we explore two different architectures of generator and discriminator, namely, simple and complex, as specified in Fig. 1. We follow the same experimental protocol in the paper, i.e. we feed source images with different labels to see if the source images’ semantic information is taken into account during the transferring procedure. The results are shown in Fig. 3(a) and Fig. 3(b). As we can see, the label domination problem occurs in both architectures. However, we find that mode collapse also appears, i.e. identical images are generated for each input label, regardless of source images. Therefore, we apply Spectral Normalization [5] to discriminator to stabilize training.

Spectral Normalization. Spectral Normalization is a weight normalization approach to stabilize the training of discriminator. It mitigates the exploding gradient and mode collapse problem by controlling the Lipschitz constant of the discriminator. Readers may refer to [5] for more detail. Trying to eliminate the effect of label domination, we substitute all normalization layers (such as batch normalization) in the discriminator with Spectral Normalization. The result is shown in Fig. 3(c). Evidently, the mode collapse problem is resolved. However, we can see that label still dominates the generation, which is not satisfactory. If not specified, all models in the paper adopt cycle consistency loss and Spectral Normalization.

4 Appendix D: Additional Results

4.1 Unlabeled data in target domain

Dataset	# of data per class	ACAL	Relaxed cGAN
$S \rightarrow \mathcal{M}$	10	93.9	94.9
$S \rightarrow \mathcal{M}$	100	91.8	97.3
$S \rightarrow \mathcal{M}$	6000	92.2*	99.1

Table 1: Experiments of unlabeled data in the target domain. The number of labeled samples per class is fixed as 10. The result marked by* is obtained in our implementation and others are from the ACAL paper [3].

We show that our jointly-training framework also makes good use of unlabeled data. We fix the number of labeled samples to be 10 for each class and increase the number of unlabeled ones. The results are summarized in Table 1. Our model’s performance continuously increases as we add more unlabeled data, indicating its effective utilization of these unlabeled samples. We mainly contribute this to the adoption of the marginal loss and the ENT loss [2].

4.2 Quality of generated images

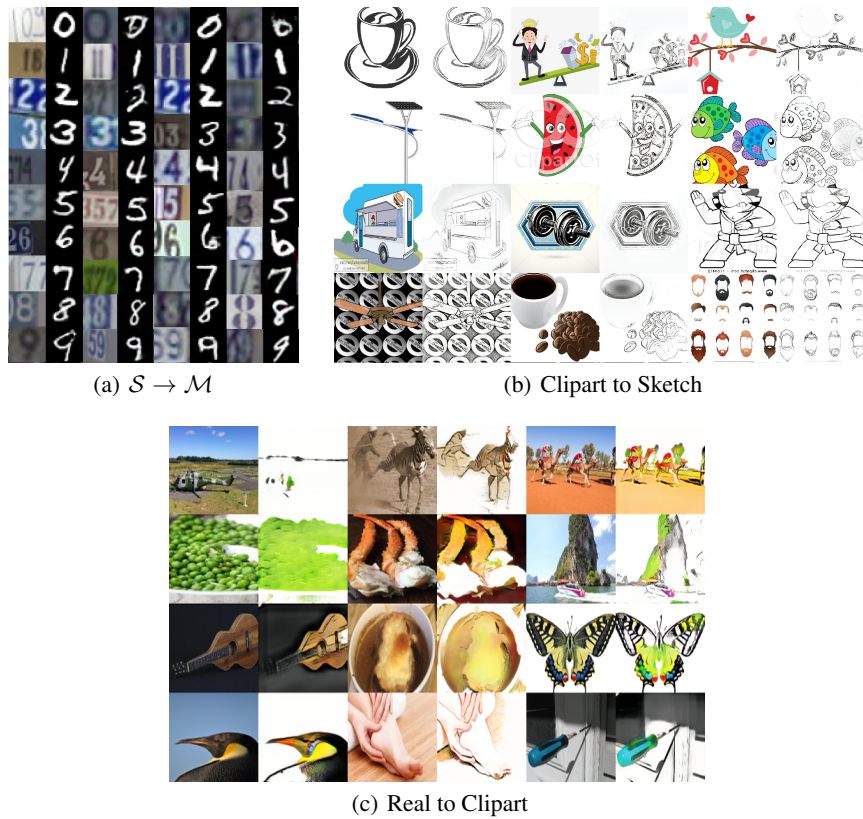


Figure 4: Visualization of $S \rightarrow \mathcal{M}$ and DomainNet generation. The odd columns are the inputs to the generator, and the even columns are the corresponding outputs.

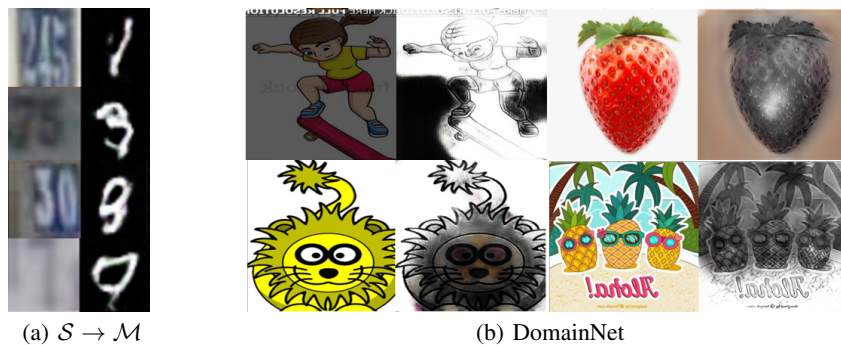


Figure 5: Visualization of some failure cases.

In the paper, we show several representative figures to demonstrate our idea. Here we put more generation results to show the diversity and output quality of Relaxed cGAN, referring to Fig. 4. We also illustrate several badly generated samples of Relaxed cGAN, as shown in Fig. 5. We take the assumption that the existence of these failure cases is mainly caused by the unstable training of GAN, which may a future direction of considering GAN training into SSDA.

References

- [1] Ian Goodfellow, Jean Pouget-Abadie, Mehdi Mirza, Bing Xu, David Warde-Farley, Sherjil Ozair, Aaron Courville, and Yoshua Bengio. Generative adversarial nets. In *Advances in neural information processing systems*, pages 2672–2680, 2014.
- [2] Yves Grandvalet and Yoshua Bengio. Semi-supervised learning by entropy minimization. In *Advances in Neural Information Processing Systems*, pages 529–536, 2005.
- [3] Ehsan Hosseini-Asl, Yingbo Zhou, Caiming Xiong, and Richard Socher. Augmented cyclic adversarial learning for domain adaptation. *arXiv preprint arXiv:1807.00374*, 1(3), 2018.
- [4] Alex Krizhevsky, Ilya Sutskever, and Geoffrey E Hinton. Imagenet classification with deep convolutional neural networks. In *Advances in Neural Information Processing Systems*, pages 1097–1105, 2012.
- [5] Takeru Miyato, Toshiki Kataoka, Masanori Koyama, and Yuichi Yoshida. Spectral normalization for generative adversarial networks. *arXiv preprint arXiv:1802.05957*, 2018.
- [6] Xingchao Peng, Qinxun Bai, Xide Xia, Zijun Huang, Kate Saenko, and Bo Wang. Moment matching for multi-source domain adaptation. In *Proceedings of the IEEE International Conference on Computer Vision*, pages 1406–1415, 2019.
- [7] Kuniaki Saito, Donghyun Kim, Stan Sclaroff, Trevor Darrell, and Kate Saenko. Semi-supervised domain adaptation via minimax entropy. In *Proceedings of the IEEE International Conference on Computer Vision*, pages 8050–8058, 2019.
- [8] Jun-Yan Zhu, Taesung Park, Phillip Isola, and Alexei A Efros. Unpaired image-to-image translation using cycle-consistent adversarial networks. In *Proceedings of the IEEE international conference on computer vision*, pages 2223–2232, 2017.